Polarization Imaging to Identify Disease Features of Gastrinoma

Julianne Chania Setiadi[1], Thomas G. Knapp[1], Justina Bonaventura[3], Juanita L. Merchant[2], Travis W. Sawyer[1,2,3]

Department of Biomedical Engineering[1], College of Medicine[2], and Wyant College of Optical Sciences[3], University of Arizona

Biomedical Optics & Optical Measurement

THE UNIVERSITY OF ARIZONA

Background

Gastrinomas are a type of gastroenteropancreatic neuroendocrine tumors found in the pancreas or duodenum causing the production of excessive levels of gastrin. Multiple endocrine neoplasia type 1 (MEN-1) is a rare autosomal-dominant disease, normally associated with a broad range of endocrine tumors, including gastrinoma. Gastrinomas in MEN-1 tend to be small, multiple and preferentially located in the duodenum[1].

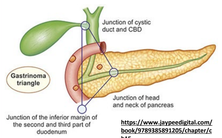

Figure 1: 90% of gastrinomas are located within the "Gastrinoma Triangle." Regions include the junctions of: (1) cystic duct and common bile duct, (2) head and neck of pancreas, and (3) the inferior margin of the second and third part of duodenum.

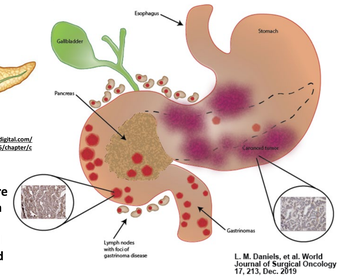

Figure 2: Illustration of gastrinoma spread within the gastrointestinal tract.

Motivation

Gastrinomas occur in one to three cases per million people in the USA annually[2], with 60 – 90% of these tumors being malignant[4]. Approximately 80% of gastrinoma are sporadic, and 20–30% percent occur in association with MEN-1[3].

There is a mean delay of 4–7 years in the diagnosis[4], and previous studies reported that the sensitivity of conventional imaging techniques for gastrinoma localization was poor, ranging only from 40–70%[7]. Surgery is curative but due to limited localization techniques, is only possible <50% of patients and nearly no patients with MEN-1 syndrome[4].

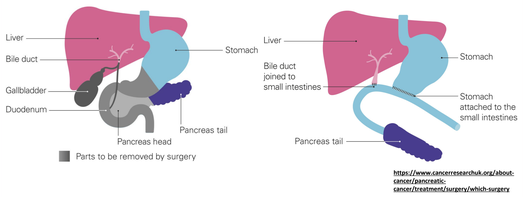

Figure 3: Surgical treatment generally includes the removal of the pancreas, duodenum, gallbladder, and part of the bile duct, liver, and stomach, resulting in excessive tissue removal[5]. This procedure is commonly known as pancreatoduodenectomy or the Whipple procedure. 5- and 10-year survival are > 90% when an isolated tumor is removed surgically, compared to 43% at 5 years and 25% at 10 years with incomplete removal[6].

We hypothesize that polarized light imaging will show contrast between healthy and cancerous duodenal tissue to identify disease features of gastrinoma. This may eventually lead to advanced imaging techniques to aid in faster diagnostic time with better tumor localization.

Methods

A custom Nikon Polarimeter was used to take Mueller Matrix Polarized Light The system was constructed through modifications of a Nikon ECLIPSE LV100N POL polarizing microscope[9]. The samples imaged are formalin-fixed paraffin-embedded (FFPE) slides of gastroenteropancreatic neuroendocrine tumors that were obtained through the University of Michigan Endocrine Oncology Repository (IRB #HUM00115310). Mueller polarimetry imaging is used due to its sensitivity to micro and nanoscale structures as predicted by scattering theory.

The Nikon Polarimeter operates in a backscattering configuration and previous studies have demonstrated that light scattering by small scatterers and light absorption are the key factors for observed polarimetric image contrast. Mueller Matrix decomposition were performed to extract polarimetric effects such as diattenuation, retardation, and depolarization. The polarimeter used captured images at 405, 442, 473, 543, and 632nm. The polarizers and waveplates were also rotated at 90-, 135-, 180-, and 225-degrees during imaging.

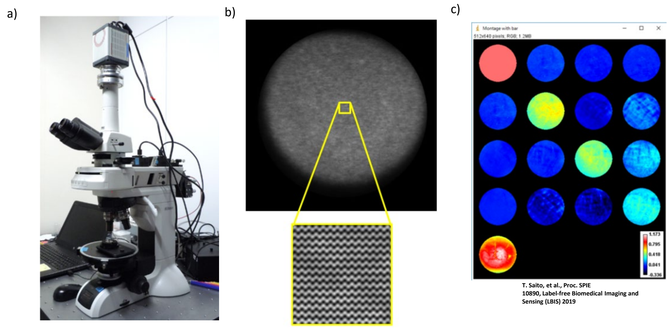

Figure 4: a) The Nikon Polarimeter used for imaging. b) Image taken exhibiting Fourier domain imaging polarimeter with polarizer at 30-degrees. c) Complete Mueller Matrix Map obtained from the instrument.

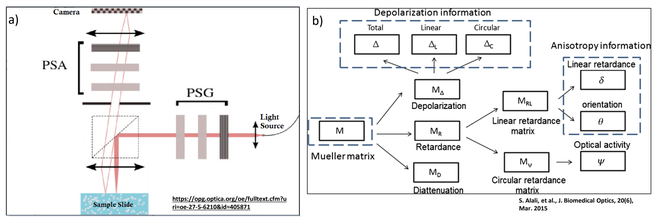

Figure 5: a) Path of light through backscattering polarimeters, which consists of a polarization state generator (PSG) and analyzer (PSA). b) Flowchart illustrating Mueller Matrix decomposition to acquire depolarization, diattenuation and retardance.

During imaging, the sample slides were tilted to minimize glare. A slide holder with a tilting wedge with hash marks were created and 3D printed to assist in tissue section imaging. The tissue samples were captured when laid flat and tilted by 1-degree using the tilting wedge (Fig. 6).

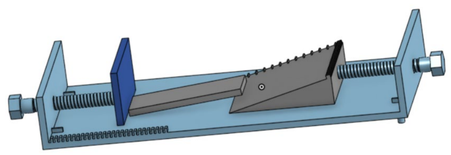

Figure 6: Adjustable slide holder with tilting wedge and hash marks. Screws were used to hold tilting wedge and slide in place.

UOM-A002-6A : Section 3 (MEN-1 Gastrinoma)

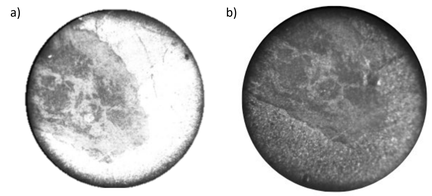

Figure 7: a) Slide sample without tilting displaying a lot of glare. b) Slide sample with tilting, minimal glare.

Images captured by the polarimeter were then compared to the H&E-stained images of the same slide to identify tissue components (Fig 8).

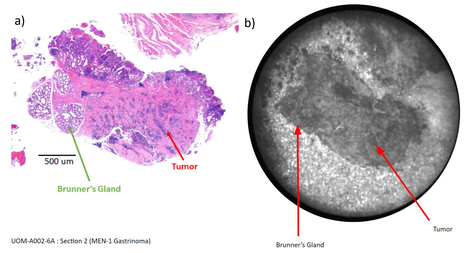

Figure 8: Comparison of H&E-stained slide (a) to polarimeter image (b) to help in tumor and Brunner's gland identification.

The analysis files generated during imaging were ran through a series of Python codes that calculates the Mueller Matrix decomposition. A set of depolarization, diattenuation, and retardance images were also generated for reference, as shown in Figure 9.

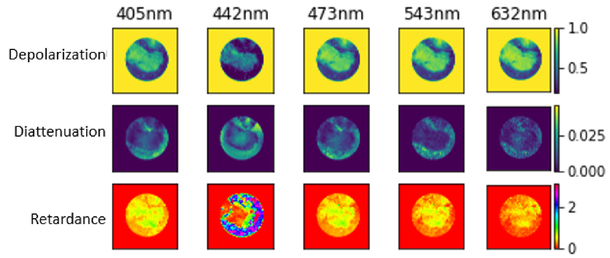

Figure 9: Images generated through Mueller Matrix decomposition to use for qualitative analysis of samples.

Using these images as a qualitative reference, masks were created on ImageJ. When running the Mueller Matrix decomposition, the masks served a purpose of only focusing the decomposition on the area within the region of interest. The average of the decomposition values were taken, and two-tailed paired t-test was done to identify significance.

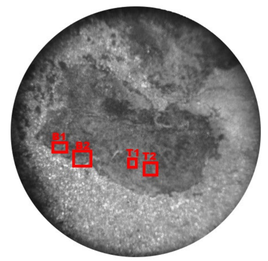

Figure 10: Masks marked the regions of interest on the image captured by the polarimeter that will undergo Mueller Matrix decomposition.

Results

The average values of the depolarization, diattenuation, and retardance, the tumor and the Brunner's gland display a similar pattern. However, the results indicate a significant difference between the average depolarization of the tumor vs. the Brunner's gland at 442, 543, and 632nm, and also the average diattenuation of the tumor vs. the Brunner's gland at 405nm. No significant difference between the retardance of the two tissues was observed. As expected, the depolarization, diattenuation, and retardance values are wavelength dependent, as shown in Table 1. Tilting of the slides shows no significant differences in the depolarization and diattenuation of the tissue but shows that there is significant difference in the retardance measurement.

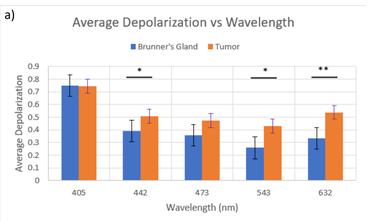

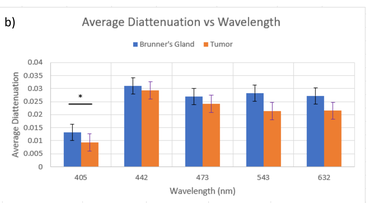

Figure 11: Bar graphs of (a) average depolarization, (b) average diattenuation, tumor and Brunner's gland slides with error bars. Two-tailed t-test is used to compare significance, which is denoted * (p<0.05), ** (p<0.01) and *** (p<0.001). We observe significant differences for depolarization at 442, 543 and 632 nm, and diattenuation at 405 nm.

Wavelength (nm)	Two-tailed T-test (p value) for Wavelength		
	Depolarization	Diattenuation	Retardance
405	X	X	X
442	5.03E-14	1.21E-07	2.10E-02
473	1.05E-08	3.07E-09	2.09E-02
543	1.26E-09	3.47E-07	9.64E-04
632	6.20E-09	2.17E-08	6.78E-11

Table 1: P values for two-tailed t-test of each wavelength to 405nm for depolarization, diattenuation, retardance. Each wavelength shows a significant difference to 405nm, confirming that the tissue characteristics are wavelength dependent.

Wavelength (nm)	Two-tailed T-test (p value) for Tilting		
	Depolarization	Diattenuation	Retardance
405	0.199	0.369	0.294
442	0.071	0.260	0.026
473	0.194	0.337	0.014
543	0.167	0.400	0.036
632	0.123	0.335	0.192

Table 2: P values for two-tailed t-test of each not tilted slides to slides tilted by 1-degree. Depolarization and diattenuation values show no significant difference to tilting, but retardance values at 442, 473, and 543nm shows values have significant differences.

Our results demonstrate that polarization imaging shows promise for tumor localization. Next steps include expanding sample pool and more advanced statistical analysis.

References

1. Plöckinger, U. "Diagnosis and Treatment of Gastrinomas in Multiple Endocrine Neoplasia Type 1 (MEN-1)" ***Cancers*** (20 January 2012).
2. https://wjso.biomedcentral.com/articles/10.1186/s12957-019-1758-6
3. https://www.uptodate.com/contents/zollinger-ellison-syndrome-gastrinoma-clinical-manifestations-and-diagnosis
4. https://www.ncbi.nlm.nih.gov/books/NBK6964/
5. https://www.cancerresearchuk.org/about-cancer/pancreatic-cancer/treatment/surgery/which-surgery
6. https://www.merckmanuals.com/professional/gastrointestinal-disorders/tumors-of-the-gastrointestinal-tract/gastrinoma
7. https://www.istage.jst.go.jp/article/endocrj/67/3/67_EJ19-0413/_html/-char/en
8. Fujii, T, et al. "Polarization Characteristics of Dark-field Microscopic Polarimetric Images of Human Colon Tissue" ***Proceedings of SPIE*** (4 March 2019)
9. Saito, T, et al. "Multispectral Mueller Matrix Imaging Dark-field Microscope For Biological Sample Observation" ***Proceedings of SPIE*** (4 March 2019)